

## **I. Late Cretaceous magmatic perturbation of the thermal-mechanical architecture of the Sevier hinterland middle crust in western Utah**

### **Introduction**

The hinterland region of the Sevier Orogen in western Utah and eastern Nevada hosts numerous Late Cretaceous leucogranite plutons with isotopic compositions that indicate they formed from nearly pure crustal melts (Barton and Anderson, 1990; Best et al., 1974; Farmer and De Paolo, 1983; Miller and Bradfish, 1980). These leucogranites often form the core of structural and deformational culminations that resemble gneiss domes. Metamorphic fabrics in these domes have commonly been interpreted as reflecting regional strain; however, many of these domes display abrupt lateral increases in metamorphism and intensification of strain in the immediate surroundings of Late Cretaceous granites. In these settings, distinguishing between regional tectonite fabrics and those related to granite emplacement is challenging, and yet the distinction is critical for regional tectonic interpretations. The role of these granite cored gneiss domes on the thermal and deformational architecture of the hinterland crust during the Late Cretaceous remains enigmatic.

The Deep Creek Range of western Utah experienced significant deformation, metamorphism, and plutonism during the Late Cretaceous and is an ideal place to investigate these problems. The range has been tilted approximately 40-50° to the west during slip on a range bounding normal fault so that paleodepth increases to the east (Rodgers, 1987), providing a cross-section of the upper to middle crust and the opportunity to investigate the interplay between pluton emplacement and deformation at different

structural levels. A domal structural culmination centered on the Late Cretaceous Trout Creek Intrusive Complex (TCIC) is characterized by an abrupt increase in metamorphic grade and strain in the country rock and has all of the trademark features of a granite cored gneiss dome. In this study, we present the results of integrated geologic mapping, microstructural analysis, and metamorphic and igneous geochronology to constrain the age of emplacement of the TCIC and its role in deformation and metamorphism in the country rock.

### **Geology of the Deep Creek Range**

The Deep Creek Range is a N-S trending mountain range on the Nevada-Utah border in the eastern Great Basin located in the heart of the Sevier hinterland, where mid- to lower-crustal thickening above an inferred west-dipping basal detachment surface accommodated east-directed thin-skinned shortening in the fold-and-thrust belt in central Utah (Figure 1a; Armstrong, 1968; DeCelles & Coogan, 2006; Miller and Gans, 1989; Taylor et al, 2000). Crustal thickening in the hinterland led to prograde metamorphism and anatexis in the lower crust, ultimately resulting in the emplacement of leucogranite plutons with isotopic compositions indicative of nearly pure crustal melts (Douce et al., 1990; Farmer and DePaolo, 1983; Lee et al., 2003; Miller and Bradfish, 1980; Wright and Wooden, 1991). Metamorphism and plutonism were geographically dispersed and diachronous but peaked in the Late Cretaceous (90-70 Ma; Camilleri and Chamberlain, 1997; Cruz-Uribe et al., 2015; Kelly et al., 2015; McGrew et al., 2000; Miller et al., 1988; Miller and Gans, 1989).

The geologic framework of the southern Deep Creek Range was laid out by Rodgers (1987), who focused on the deformational and thermal history and provided important

context for this project. The eastern Deep Creek Range is underlain by the Neoproterozoic Trout Creek and McCoy Creek groups, composed of interbedded quartzite, metapelitic schist, metadiamictite, and minor marble. The western part of the range is underlain by upper-crustal Paleozoic carbonates and Eocene volcanic rocks (Figure 1b and c). The Eocene Ibapah pluton intrudes the older succession in the central part of the range and has a narrow contact metamorphic aureole that overprints penetrative cleavages that are

interpreted to have formed during the Cretaceous. The first is reflected in a west dipping cleavage ( $S_1$ ) that is also present in many other nearby ranges and is interpreted to have formed as a result of east directed layer parallel shear (Miller et al., 1988; Rodgers, 1987). During the second event, rocks on the southern flank of the range were folded into the Water Canyon Anticline, a large recumbent fold that closes to the west and has a gently north plunging fold axis. A locally developed cleavage ( $S_2$ ) that appears to be axial planar to the

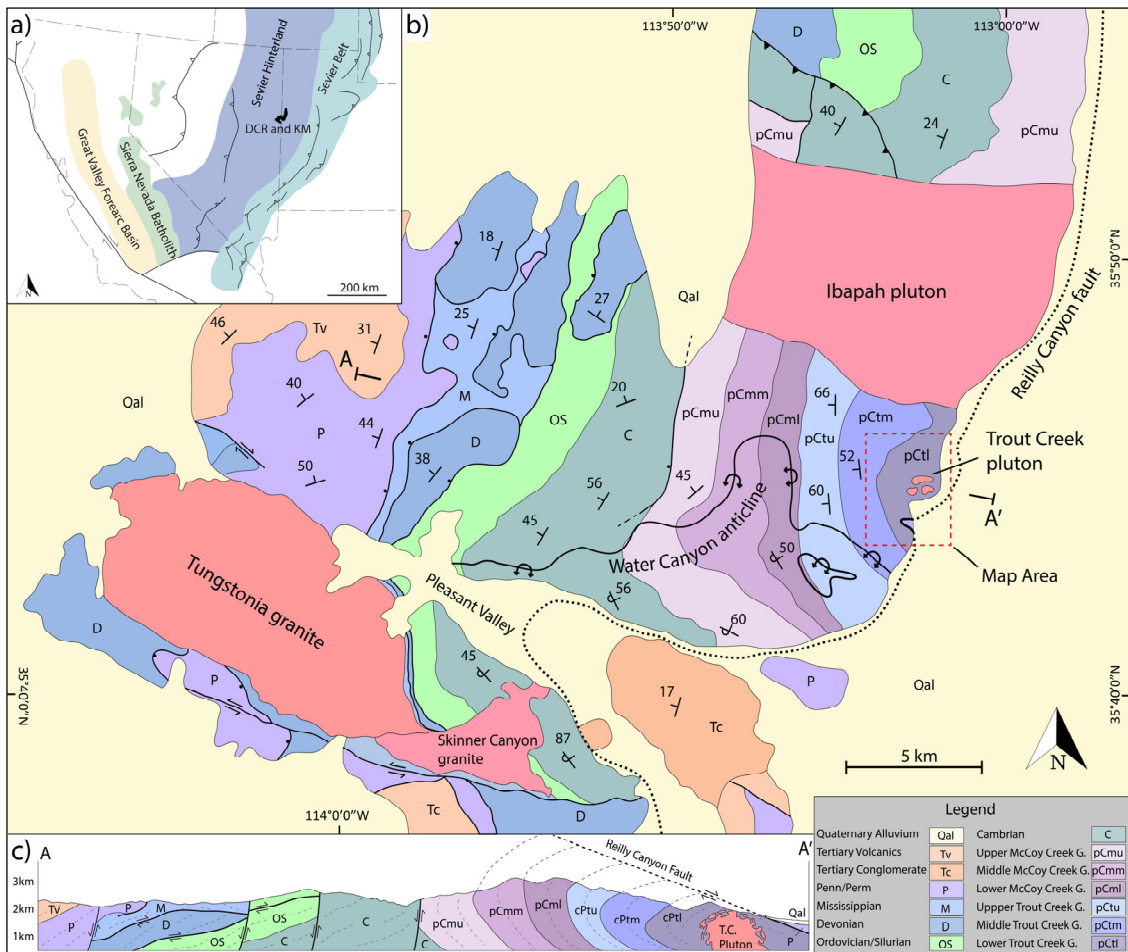


Figure 1: a) Simplified tectonic map of a portion of the western U.S. showing the location of major tectonic features of the Sevier orogen. The Deep Creek Range is located on the Nevada-Utah border and lies within the hinterland of the Sevier orogen approximately 100 km west of the frontal portion of the fold-and-thrust belt (modified from DeCelles and Coogan, 2006). b) Simplified geologic map of the Deep Creek Range and Kern Mountains based on mapping by Hose and Blake (1976), Rodgers (1987), and Nutt and Thorman (1994). c) Simplified WNW-ESE cross section across the southern Deep Creek Range based on mapping by Rodgers (1987) and Nutt and Thorman (1994).

Water Canyon Anticline also developed during this event. Metamorphism increases down section from unmetamorphosed Paleozoic carbonates in the west to upper greenschist grade within the stratigraphically lowest units and locally to amphibolite grade in several metamorphic culminations. The Trout Creek culmination, and associated Trout Creek pluton, are situated at the deepest exposed structural levels on the eastern flank of the range and are the primary focus of this study (Figures 1 and 2).

### **Geology of the Trout Creek Culmination**

Rodgers (1987) briefly discusses the Trout Creek area and speculated that the doming and increase in deformation and metamorphism was a result of pluton emplacement. Three weeks of field study for this project built upon his work by mapping contacts in greater detail, collecting a dense array of bedding and cleavage orientations, and sampling key units for petrographic and geochronologic analysis. This new work is illustrated in a detailed map of a ~15 km<sup>2</sup> area centered around the Trout Creek pluton, as well as two perpendicular cross sections across the map area (Figures 2 and 3).

The Trout Creek intrusion consists of a medium- to fine-grained leucogranite that intrudes the basal schist member of the ~4500 m thick Trout Creek Group (Figure 4a). The

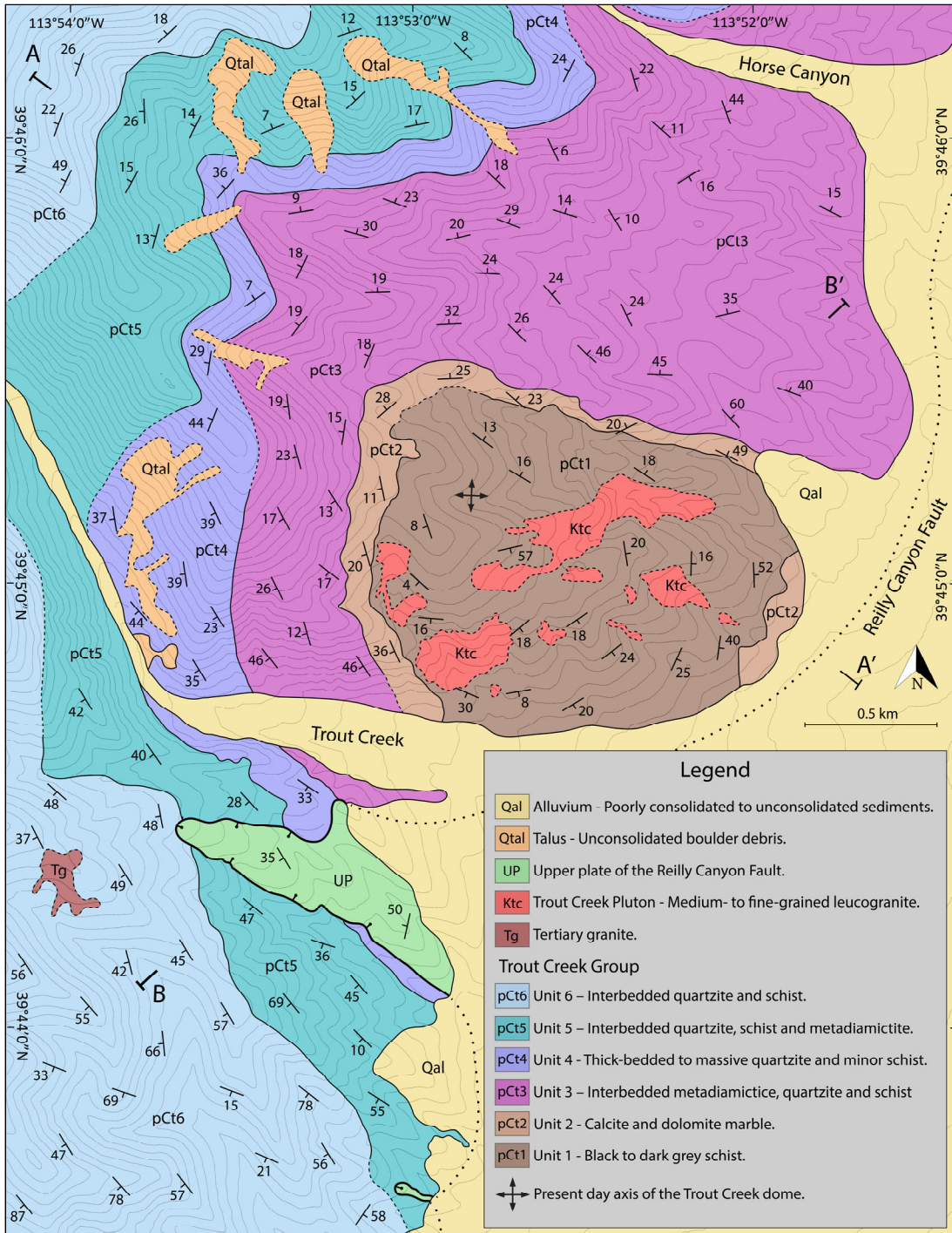


Figure 2: Geologic map of the Trout Creek culmination.

exposed pluton isn't composed of a single body, but instead is exposed over a ~2 km<sup>2</sup> area as abundant dikes and sills (not shown in Figure 2) that radiate from several small stocks,

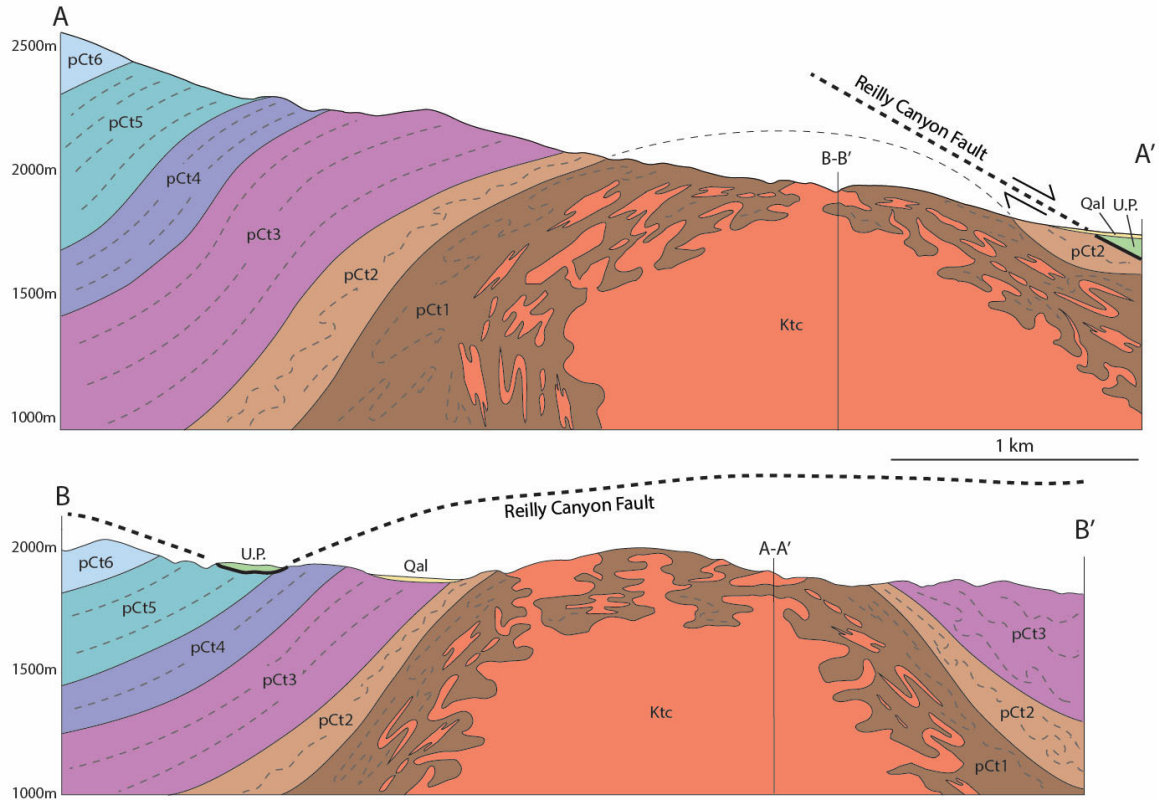


Figure 3: Mutually perpendicular cross sections along lines A-A' (NW-SE) and B-B' (SW-NE) on the geologic map. Both cross sections have a similar geometry, highlighting the fact that the culmination has a domal and not cylindrical geometry. However, A-A' is approximately perpendicular to the axis of Cenozoic tilting of the range and therefore the geometry of the culmination when it formed during the Cretaceous is tilted to the west.

and will hereafter be referred to as the Trout Creek Intrusive Complex (TCIC). Bedding and both the S<sub>1</sub> and S<sub>2</sub> foliations dip gently to moderately away from the TCIC, forming a structural dome that is at least 5 km in diameter. Projection of unit contacts above the dome indicates that the dome has approximately 1-1.5 km of structural relief. The degree of penetrative deformation in the country rock increases markedly in the vicinity of the TCIC, grading over a distance of ~500 m from quartzites and phyllite with only weakly developed cleavages in shale beds and well-preserved sedimentary structures in quartzites, to highly strained tectonites with an intense transposition of foliation in the lower half of pCm3 and

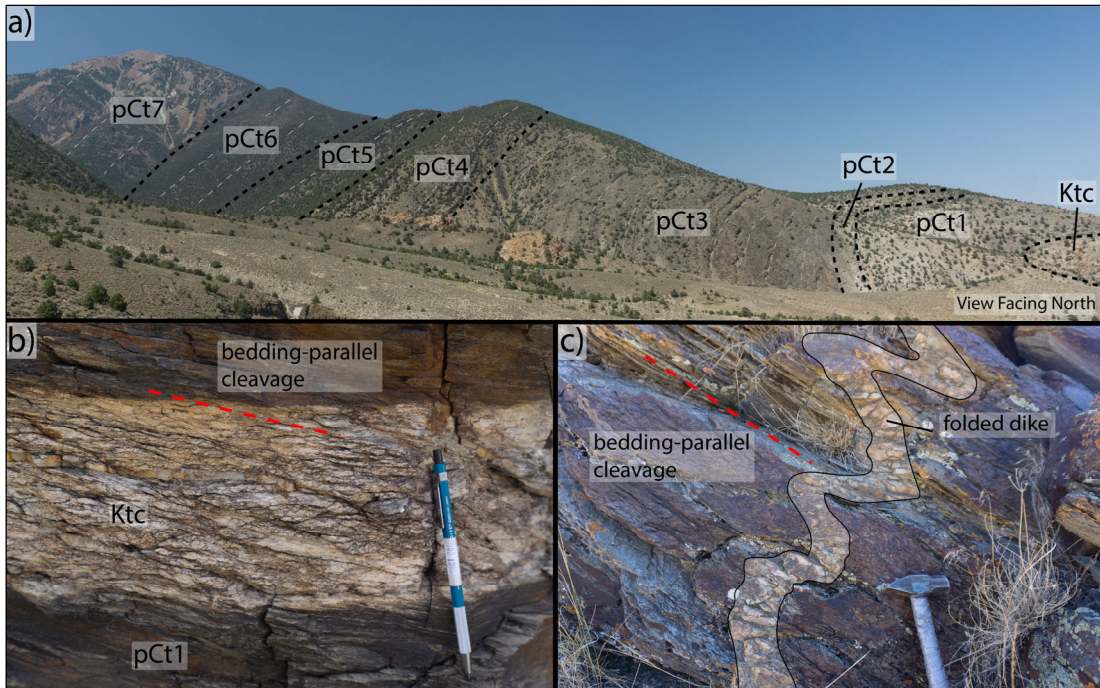


Figure 4 a) View north across Trout Creek Canyon showing the approximate contacts of the Trout Creek Group units (pCt1-pCt7) and the TCIC (Ktc). Bedding in general dips to the west in this part of the range and moves upsection westward towards the crest of the range, which is underlain by the uppermost unit of the Trout Creek Group. Distance across the field of view of the photo is approximately 8 km. b) Sill from the TCIC with a well-developed foliation that is continuous with the country rock. c) Folded TCIC dike with an axial surface approximately parallel to the bedding-parallel cleavage.

below. Metamorphic grade also increases within a few hundred meters of the TCIC from greenschist facies phyllite and fine-grained biotite-muscovite schist to amphibolite facies coarse-grained schist with conspicuous large porphyroblastic biotite, garnet, andalusite, and staurolite irregularly distributed within the basal schist (pCt1).

Two cleavages are present in schistose horizons of units 3, 5 and 6 of the Trout Creek Group in the periphery of the domal culmination. The first cleavage ( $S_1$ ) is consistently more west dipping than bedding with an intersection angle of approximately 20–40° (Figure 5). This relationship with bedding is consistent around all sides of the culmination, suggesting that the cleavage formed prior to the development of the structural

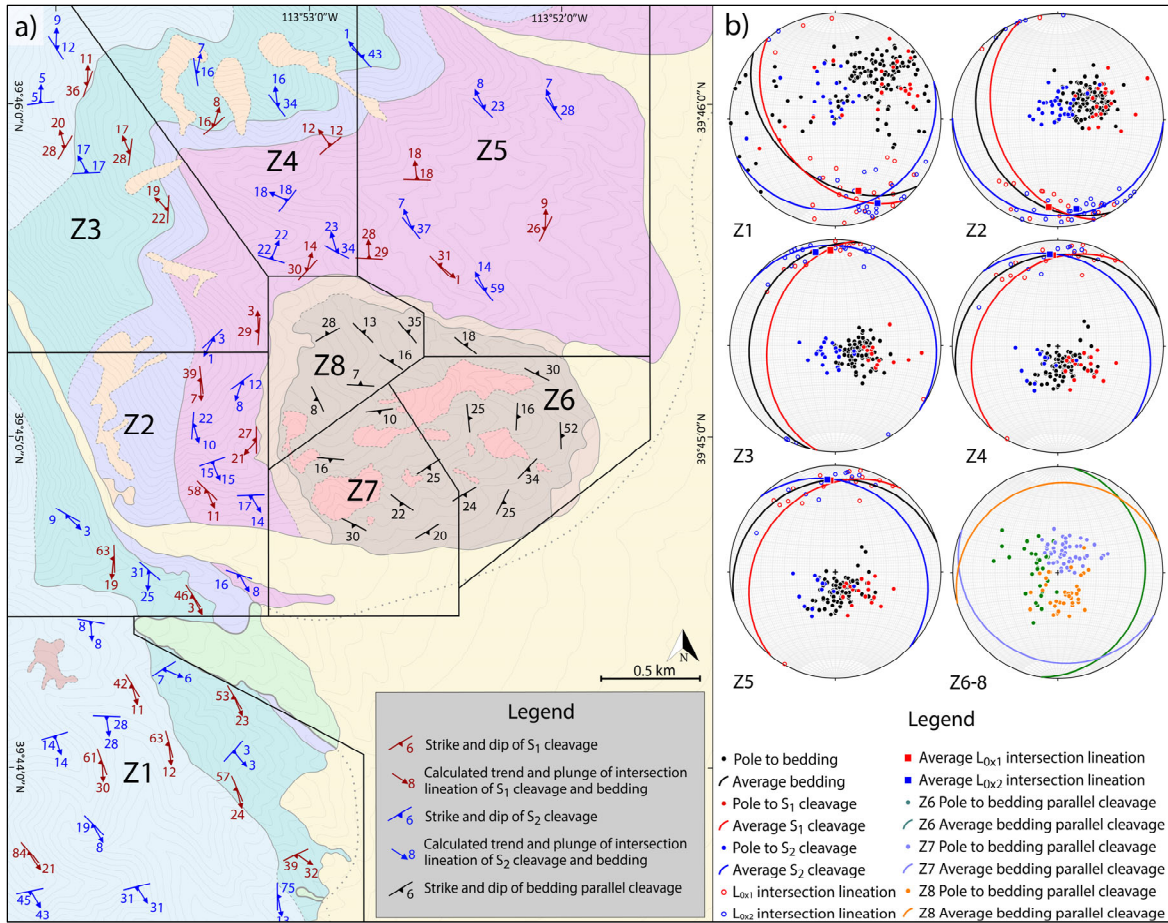


Figure 5: a) Map showing the orientations of the  $S_1$ ,  $S_2$  and bedding parallel cleavages and their intersection lineations with bedding.  $S_1$  is consistently more west dipping than bedding and in general dips away from the Trout Creek pluton. The  $L_{0x1}$  intersection lineation plunges gently to the NNW in the northern half of the map area and to the SSE in the southern half.  $S_2$  typically dips gently to moderately away from the center of the dome, with an  $L_{0x2}$  intersection lineation that plunges gently to moderately to the north to northwest in the northern half of the map area and to the south to southeast in the southern half. b) Zoned stereonets showing the orientations of poles to bedding,  $S_1$ ,  $S_2$  and the bedding parallel cleavage as well as calculated intersection lineations.

dome and was passively rotated during doming. This cleavage is widespread through the southern Deep Creek Range and increases in intensity and metamorphic grade from a spaced slaty cleavage in stratigraphically higher units near the crest of the range, to a penetrative biotite-grade schistosity in the deepest stratigraphic levels. A similar west-dipping cleavage is present in many of the surrounding ranges and thus appears to reflect a relatively

widespread deformational event in the Sevier hinterland (Miller et al., 1988, Miller and Gans, 1989). Previous workers interpreted this cleavage to be a result of east directed layer parallel shear when the section was approximately flat lying based on the observations that 1) the cleavage is consistently more west dipping than bedding and generally intersects bedding at an angle of less than 45 degrees, 2) the cleavage becomes more well developed and the intersection angle with bedding decreases with depth, and 3) folds associated with the cleavage are rare, suggesting that bedding was never in the shortening field (Miller et al., 1988; Miller and Gans, 1989; Rodgers, 1987).

The second cleavage ( $S_2$ ) crenulates  $S_1$  and generally dips east with respect to bedding, with an intersection angle of 15-45 degrees (Figure 5). This cleavage is only present at deeper structural levels in the Deep Creek Range and was interpreted by Rodgers (1987) to be an axial planar cleavage to the Water Canyon Anticline. However, second cleavages are sporadically developed in different parts of the range and may have developed at different times and have different origins. Within the Trout Creek culmination, the second cleavage dips away from exposures of the TCIC and is generally more gently dipping than bedding, suggesting it was at least partially developed prior to emplacement of the TCIC and was passively rotated during doming. However, it also increases in intensity and metamorphic grade in the vicinity of the TCIC within pCt3 and below, suggesting that it was actively developing during the time of emplacement and was upgraded due to the thermal effects of the magmas. In the basal micaceous schist unit of the Trout Creek sequence, there is a single very well-developed foliation that is parallel to bedding and contains numerous isoclinal folds with axial surfaces parallel to the foliation. It appears that the additional strain in the basal schist likely transposed bedding,  $S_1$  and (early)  $S_2$  into parallelism to form a

single penetrative foliation. This foliation forms the core of the dome and is subhorizontal at the dome axis and dips gently to moderately away from the dome around its margins (Figure 5). It is unclear whether this high-strain transposition foliation is an entirely new cleavage or simply an intensification of the S<sub>2</sub> cleavage described above.

The age of the penetrative strain and strain intensification appears closely related to the emplacement of the TCIC. Although the larger stocks appear undeformed, their margins have a well-developed deformational fabric that is continuous with and parallel to the fabric in the country rock (Figure 4b). Additionally, dikes and sills that radiate from the pluton are folded and boudinaged (Figure 4c). The lack of deformation in the interior of the stocks is likely due to the rheological contrast with the country rock, such that strain was strongly partitioned into the schist. The close spatial association of the highest strain rocks with the TCIC and the variable strain observed in the TCIC suggest the TCIC and high strain deformation were broadly synchronous. The highest intensity fabrics have a very well-developed foliation, but lineations are either absent or very weakly developed, suggesting strain was primarily in the flattening field.

### **Microstructures and Metamorphic Assemblages**

Twenty-eight oriented samples of schist from Trout Creek Group units 1, 3, 5 and 6 were collected and examined petrographically to characterize deformational fabrics, metamorphic assemblages, porphyroblast-cleavage relationships and recrystallization mechanisms. These samples range from micaceous quartzite to pelites and contain varying proportions of quartz, muscovite, biotite and chlorite. More pelitic horizons near the base of pCt3 and pCt1 contain porphyroblasts of garnet ± andalusite ± staurolite.

The  $S_1$  cleavage is best developed in pelitic horizons in Trout Creek units 3, 5, and 6 and is absent in the intervening quartzite units. It is defined by fine-grained syn-kinematic biotite and muscovite, which is partially retrograded to chlorite, as well as a weak grain or aggregate shape preferred orientation of quartz (Figure 6b). Sparse, small garnets in pCt3 have trails of quartz and oxide inclusions continuous with  $S_1$ , suggesting syn- to post-kinematic growth, however this relationship is obscured by  $D_2$  deformation. The presence of synkinematic biotite and possibly garnet suggests that this cleavage formed at upper greenschist to lower amphibolite facies in this part of the range.

In the distal parts of the Trout Creek dome,  $S_2$  is a spaced cleavage defined by distinct bands of aligned biotite, muscovite and chlorite and insoluble concentrations of oxides along dissolution seams (Figure 6b). Here, rocks appear only weakly strained and sedimentary structures in many outcrops are still recognizable. The  $S_2$  cleavage domains are spaced 200-400 um apart and separate quartz-rich microlithons that preserve the  $S_1$  cleavage. The growth of micas along dissolution seams suggests that the cleavage began to form by crenulation of the  $S_1$  cleavage and dissolution/precipitation of quartz along the cleavage domains, followed by new mica growth at a higher metamorphic grade. In the lower portions of pCt3 in the vicinity of the TCIC, the  $S_2$  cleavage is better developed and defined by penetrative mica growth, largely obscuring the  $S_1$  cleavage (Figure 6c). Cleavage domains of  $S_2$  are still recognizable but more closely spaced and overprinted by penetrative mica growth. In outcrop, these rocks appear progressively more flaggy and strained from the middle of pCt3 toward its base, with sedimentary structures becoming unrecognizable.

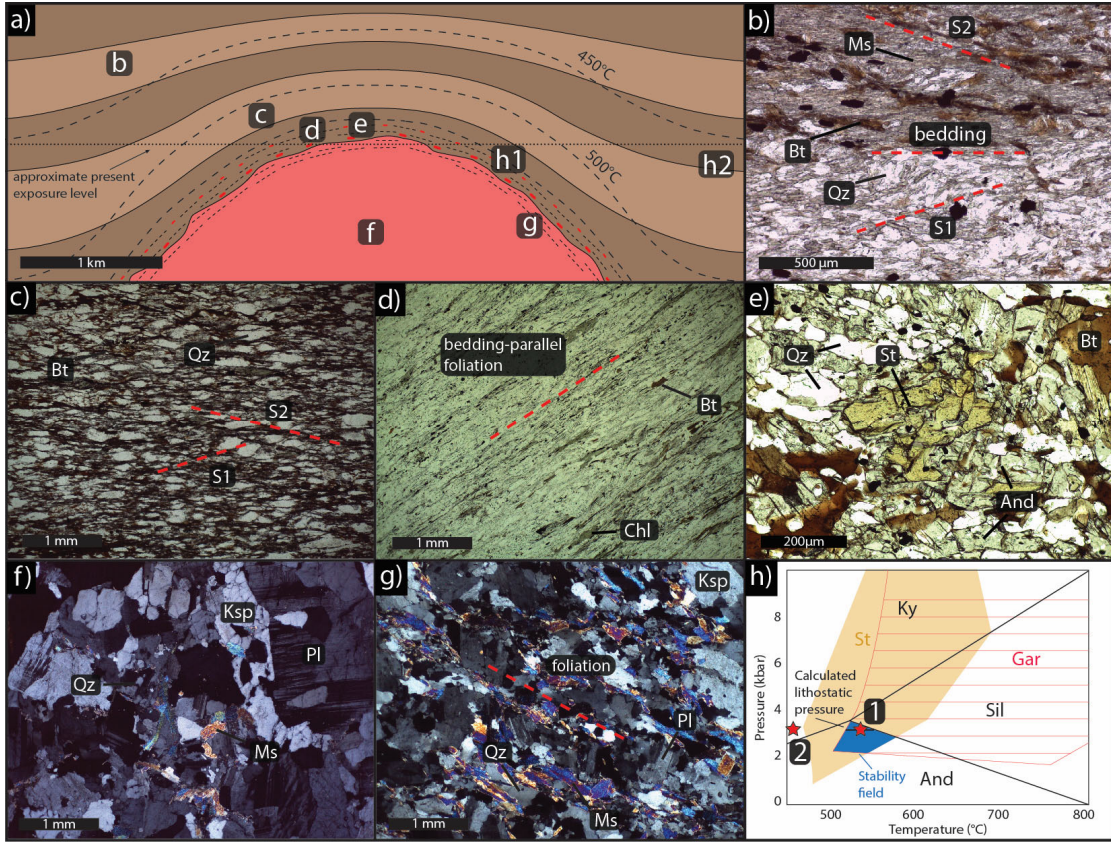


Figure 6: a) Schematic cross section of the Trout Creek culmination during the Late Cretaceous showing doming of the country rock, elevated isotherms, and the approximate present exposure level. The high strain fabric along the pluton margins is shown schematically as dashed lines and metamorphism is shown as red rectangles. b) Photomicrograph with a view facing north showing bedding, S<sub>1</sub> and S<sub>2</sub>. S<sub>1</sub> dips toward the west (left) and is defined by aligned muscovite which is most obvious in the lower half of the image and in the upper half within microlithons of the S<sub>2</sub> cleavage. The S<sub>2</sub> cleavage dips to the right (east) and is a spaced cleavage defined by cleavage domains of aligned synkinematic biotite (PPL). c) Sample from pCt3 showing a very well developed S<sub>2</sub> cleavage (PPL). d) High-strain bedding parallel foliation in pCt1 defined by highly aligned micas and a grain shape preferred orientation in quartz (PPL). e) Sample from pCt1 with porphyroblastic biotite, staurolite, and andalusite (PPL). f) Undeformed TCIC leucogranite from the interior of the stock. g) Deformed TCIC leucogranite from the margins of a dike. h) P-T diagram showing the stability fields of garnet, staurolite and the aluminosilicates. The assemblage of garnet+staurolite+andalusite in the Trout Creek schist indicates pressures of ~2-3.8 kbar and temperatures of ~500-600°C (stability field shown in blue). Calculated lithostatic pressure for a 13.5 km section of rock with an average density of 2.6 g/km<sup>3</sup> shown as horizontal line in the blue stability field for the assemblage.

The basal schist of the Trout Creek Group is highly strained with a single well-developed bedding-parallel penetrative cleavage defined by aligned micas and a grain and aggregate shape preferred orientation in quartz (Figure 6d). In outcrop, these rocks are

flaggy and sedimentary structures have been completely overprinted by deformation. The additional strain within this unit obscured S<sub>1</sub>-S<sub>2</sub> relations by transposing them into parallelism with each other and with bedding. Conspicuous porphyroblastic garnet, biotite, andalusite and staurolite are irregularly distributed in close proximity to the TCIC. Garnet typically occurs as 1-2 mm porphyroblasts that are partially to completely replaced by post-kinematic sericite or chlorite. Cores have fine-grained inclusions that make them appear “dirty” whereas the rims are clear, suggesting two stages of growth or a change in reaction during a single stage of growth. Micas are aligned with the foliation and present in strain shadows of garnet porphyroblasts, indicating synkinematic growth of mica and pre- to synkinematic garnet growth. In some samples there is also decussate biotite that cuts the foliation, indicating post-kinematic static growth. Andalusite occurs as porphyroblasts up to ~2 cm across with strain fabric-parallel quartz inclusions, suggesting syn- to post-kinematic growth (Figure 6e). Andalusite pseudomorphs composed of fine-grained micas and quartz up to 5 cm across are more common and indicate that andalusite was widespread within pCt1. Staurolite occurs as 100-500 um porphyroblasts but the timing of growth is ambiguous (Figure 6e). Quartz occurs as weakly aligned aggregates with equant to slightly elongate grains exhibiting polygonal grain boundaries suggestive of static recrystallization. The highly variable quartz grain-size and similar extinction angle of adjacent subgrains suggests that subgrain rotation recrystallization was dominant. However, pinning structure between micas and quartz was also observed, suggesting a component of grain boundary migration.

The Trout Creek pluton is largely undeformed in its interior but has a well-developed foliation around its margins and in dikes and sills that is continuous with the country rock

(Figures 6f and 6g). The foliation decreases in intensity with distance from the pluton margins and is defined by aligned muscovite and a grain-shape preferred orientation in quartz. Feldspar is relatively undeformed except for moderate deformation twinning and minor recrystallization around grain boundaries, indicating that the majority of strain was partitioned into the quartz and micas.

Textural relationships between porphyroblasts and the deformational fabric and their spatial coincidence suggests that peak metamorphism occurred during the formation of the high strain fabric in the basal unit of the Trout Creek Group. The presence of garnet, andalusite and staurolite indicates that peak P-T conditions were between ~2-3.8 kb and ~500-600°C (Figure 6h; Spear, 1993). Additionally, the dominant recrystallization mechanism observed in quartz is subgrain rotation with minor grain boundary migration, suggesting temperatures of approximately 500-550°C (Hirth and Tullis, 1992). Pressures of ~2-3.8 kbar require no burial beyond the stratigraphic depth for the lower Trout Creek Group; using a stratigraphic depth of 13.5 km and an average rock density of 2.7 g/cm<sup>3</sup>, the pressure would be ~3.6 kbar, in the upper part of the stability field. Temperatures of 500-550°C at this depth would require an average geothermal gradient of approximately 35-40°C/km, which is quite high even for orogenic systems. It is more likely that the increase in temperature is localized around the TCIC and is a direct result of heat from the magma itself, rather than a regionally elevated geothermal gradient.

## **U-Pb Geochronology**

### *Methods*

U-Pb geochronology was performed on zircon from the main phase of the TCIC and monazite from the basal unit of the Trout Creek Group using the Laser-Ablation Split-Stream facility at UC Santa Barbara following the methods described in Kylander-Clark et al. (2013). Zircon crystals from a sample of the TCIC were separated using standard magnetic and density techniques, mounted on an epoxy puck, and imaged using the cathodoluminescence detector on UCSB's FEI Quanta 400F field emission source SEM prior to analysis. Monazite was analyzed in thin section to evaluate the petrographic context of mineral growth and stability. Unfortunately, grains were too small (<15um) for EPMA mapping or to perform multiple analyses per grain. Samples were ablated with a Photon Machines Excite 193 nm excimer laser using a spot size and repetition rate of 24  $\mu\text{m}$  and 4 Hz, and 8  $\mu\text{m}$  and 3 Hz for zircon and monazite respectively. U-Pb isotopes were measured with a Nu Instruments Plasma HR multi-collector ICP for both zircon and monazite, and element concentrations for monazite were measured concurrently using an Agilent 7700X quadrupole ICPMS . The primary reference material (RM) for zircon U-Pb was 91500 (Wiedenbeck et al., 1995) and GJ1 (Horstwood et al., 2016) and Plešovice (Sláma et al., 2008) were employed for accuracy and yielded ages within 2% of their expected values. Monazite 44069 was used as the primary RM for U-Pb normalization and Bananiera (Palin et al., 2013), FC-1 (Horstwood et al., 2003) and Trebilcock (Tomascak et al., 1996) yielded U-Pb ages within 2% of their expected values. Bananiera (Kylander-Clark et al., 2013) was used as the primary trace-element RM, assuming 12.9% P in monazite. Twenty-seven spot analyses were performed for zircon and a final age was calculated from a single population of nine ages. Spot analyses on fifty-one monazite grains were performed. Isotope data was reduced using Iolite software and plotted with Isoplot software (Paton et al., 2011).

## *Results*

Prior to this study, the TCIC and associated amphibolite-facies metamorphism had no credible age constraints. Rodgers (1987) performed  $^{40}\text{Ar}/^{39}\text{Ar}$  analyses on muscovite and microcline from the TCIC that yielded ages of 25-29 Ma and 17-26 Ma, respectively. However, these ages reflect final cooling of these minerals to temperatures of  $<350^\circ\text{C}$ , not the crystallization or metamorphic age. Our new U-Pb analysis of zircon from the interior of one of the large stocks indicates a crystallization age of  $80 \pm 2$  Ma, calculated from a single population of nine concordant analyses (Figure 7a; Monroe et al., 2023a). Older Mesozoic and Proterozoic ages (not shown in diagram) are interpreted to be inherited and the two younger ages are interpreted to be due to minor lead loss.

Metamorphic monazite from the Trout Creek schist yielded a wide range of 207-corrected ages between ca. 100–38 Ma (Figure 7b and 7c; Monroe et al., 2023b). Although this may suggest multiple (re)crystallization events or prolonged (re)crystallization, a cluster of dates at  $\sim 80$  Ma suggests peak metamorphism at approximately the same time as pluton emplacement. The presence of two small bodies of  $\sim 39$  Ma granite in the map area as well as the nearby much larger  $\sim 39$  Ma Ibapah pluton suggests that the  $\sim 39$  Ma monazite ages may reflect an important Eocene reheating event. It is possible that the intermediate ages reflect mixed analyses between older ( $\sim 80$  Ma) cores and Eocene rims in a single laser spot. The peak of ages at  $\sim 58$  Ma appears to be statistically significant and may represent a (re)crystallization event whose significance is unclear. The REE profile for all the monazite analyses is typical for metamorphic monazite and the depletion of the HREEs indicates garnet stability during monazite growth (Figure 7d).

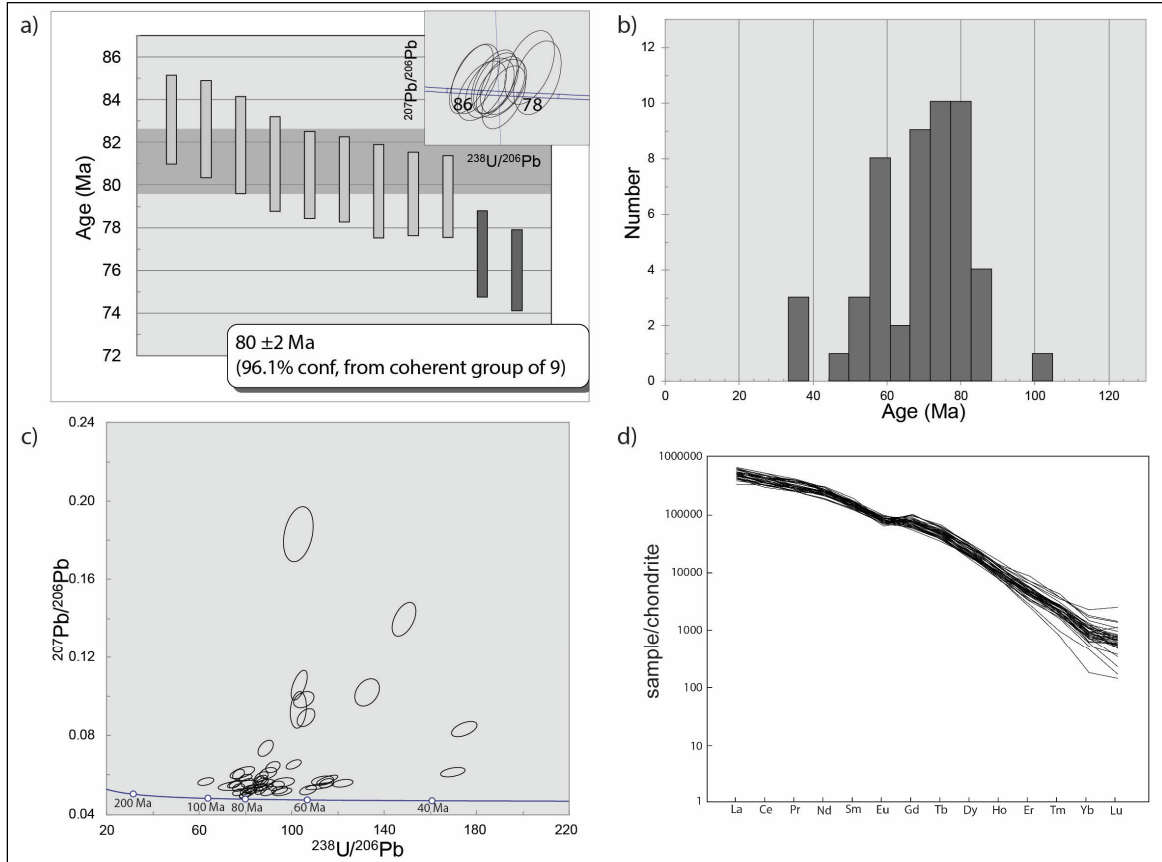


Figure 7: a) Plot showing the ages with errors of individual zircon analyses. Light grey bars represent ages that fit within a single population and were used in the final age calculation. Terra-Wasserberg concordia diagram (inset) shows that all U-Pb ratios are concordant. b) Histogram showing the distribution of monazite ages obtained from analysis of the Trout Creek schist. c) Terra-Wasserberg concordia plot of the monazite analyses showing a wide range of concordance values. d) REE plot from the monazite showing a depletion in HREEs indicating monazite growth in the presence of garnet.

## Discussion

The structural and geochronological data gathered from the Trout Creek culmination permits a reinterpretation of the timing and nature of metamorphism. The regionally developed S<sub>1</sub> cleavage that dips more westward than bedding is present throughout the culmination but does not appear to be upgraded near the TCIC and is interpreted to have formed prior to doming and the emplacement of the TCIC. A second cleavage that generally

dips more eastward with respect to bedding was upgraded in the vicinity of the TCIC and is interpreted to have been actively forming during doming. In the core of the dome, the two cleavages and bedding are transposed into a single high-strain amphibolite facies fabric. This zone of upgraded metamorphism and high strain is pervasively intruded by the TCIC, which is characterized by abundant folded and boudinaged dikes and sills with a tectonite fabric that passes continuously into the country rock. Thus, it appears that metamorphism, development of the high strain fabric and doming of the country rock occurred approximately synchronously with intrusion of the ~80 Ma TCIC. Further evidence to support this interpretation comes from the U-Pb geochronology data that indicates monazite growth in the schist began at approximately the same time as crystallization of TCIC. Thus, we conclude that emplacement of the TCIC was the primary cause of structural doming, localization of fabrics and increased metamorphic grade.

When a pluton is emplaced in the crust, space must be made to accommodate the additional volume of the ascending magma body (e.g. Hutton, 1996). Some of the hypothesized mechanisms for creating this space include fracturing and diking, stoping, ductile flow, folding of the country rocks, and tectonic accommodation along faults or ductile shear zones (e.g. Clemens and Mawer 1992; Glazner, 2004; Paterson and Farris, 2008; Paterson and Fowler 1993; Miller and Paterson, 1999). Ductile emplacement mechanisms are more likely to dominate at mid-crustal levels. In the case of the TCIC, the space occupied by the intrusion appears to have been accommodated by a combination of doming of its roof rocks and ductile flow immediately above and along the margins of the intrusion. The structural dome surrounding the TCIC has a diameter of at least 5 km with

~1-1.5 km of structural relief which could accommodate an estimated  $\geq 6$  km<sup>3</sup> of additional space. We suggest that the exposures of the TCIC at the surface are small bodies near the roof of a larger pluton at depth, as illustrated in Figure 3. Thermal rheologic weakening within the metamorphic aureole appears to have helped localize strain to within ~500 m of the TCIC and allowed for the pluton to more easily deform the country rock during emplacement. Although it is apparent that doming and ductile attenuation occurred above the roof of the pluton, it is unclear what mechanisms dominated along its sides and lower margins as only the uppermost parts of the pluton are exposed at the current level.

#### *Impact of Late Cretaceous plutons on the Sevier hinterland*

The TCIC is one of many Late Cretaceous leucogranites in the Sevier hinterland and provides a striking example of how plutons can affect the deformational and thermal architecture of their surroundings (Figure 8). Heat and fluids advected from depth by the ascending magma body resulted in elevated temperatures and strain localization at relatively shallow levels in the crust. Isotherms which are commonly thought to be horizontal apparently had significant topography, resulting in high lateral thermal gradients. In the Trout Creek culmination, background temperatures are estimated to have been ~400°C, but were upgraded to 550-600°C in the vicinity of the pluton. The complex strain field in the vicinity of the TCIC resulted from superposition of tectonite fabrics related to regional shortening and the local effects associated with pluton emplacement. Although the Trout Creek culmination is a relatively small-scale case, there are numerous other larger Cretaceous leucogranites in the Sevier hinterland that show a similar intensification of strain and metamorphism, including the ~71 Ma Tungstonia granite in the Kern Mountains (Best

et al., 1974; Gottlieb, et al., 2022) and the  $94 \pm 2$  Ma Lexington Creek pluton in the Southern Snake Range (Gottlieb et al., 2022; Lee and Christiansen, 1983). Exposures of high strain dynamothermally metamorphosed rocks such as are exposed in the vicinity of the TCIC would, in isolation, likely be interpreted as a product of a regional Barrovian metamorphic and deformational event, not the local deformational and thermal effects of a nearby pluton.

This study emphasizes the need for caution in making “tectonic” interpretations from rocks that may instead be recording very local thermal and structural events.

#### *Effect of fluids during pluton emplacement*

One of the puzzles of the metamorphic culminations in the

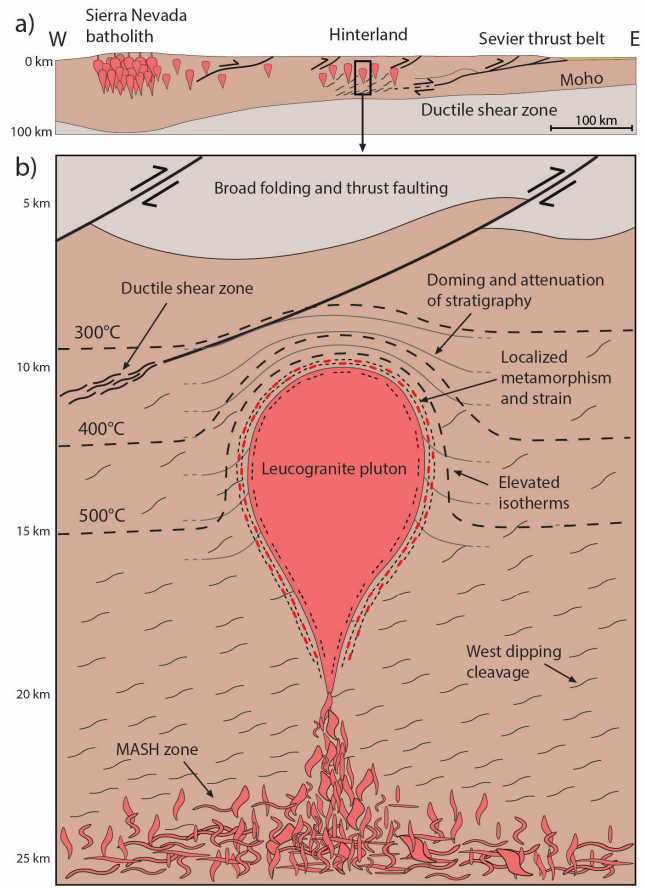


Figure 8: a) Schematic E-W cross section across the Sevier orogen during the Late Cretaceous showing the location of the hinterland region relative to the magmatic arc and the fold-and-thrust belt. Approximate area of cross section b shown as the black box. b) Schematic cross section of the Sevier hinterland during the Late Cretaceous highlighting the impacts of plutons on the thermal and deformational architecture of the crust. Isotherms have significant topography and are closely spaced around leucogranite plutons that are being intruded at different depths in the crust. Emplacement of these plutons causes localized strain and metamorphism around their margins and can result in doming of the country rock. These complex deformational and thermal structures are superimposed on an area undergoing more regional deformation associated with E-W shortening, reflected in the west dipping cleavage at deeper crustal levels and broad folding and thrust faulting at shallower crustal levels.

Sevier hinterland is that they are commonly associated with Late Cretaceous plutons; Jurassic and Eocene plutons in the same areas and at the same inferred structural depths typically only have narrow static metamorphic aureoles, even for intrusions that are much larger than the TCIC and were emplaced at the same structural/stratigraphic depth (Miller et al., 1988). *Why do some plutons have such profound effects on their country rocks while others appear to have very little? What was different during the Cretaceous that tended to produce granite cored metamorphic and deformational culminations?*

The Late Cretaceous plutons of eastern Nevada are all 2-mica leucogranites with an isotopic composition that suggests they are nearly pure crustal melts (e.g. Best et al, 1974; Miller and Bradfish, 1980; Wright and Wooden, 1991). These rocks were largely derived from the prograde metamorphism and melting of sedimentary rocks which would result in magmas with a high volatile content. More speculatively, these magmas were likely rising in concert with fluids released from dehydration reactions in the zone of prograde metamorphism. The presence of abundant fluids associated with the rise of these magmas would have drastically reduced rock strength as well as increased diffusivity and decreased nucleation rates, allowing rapid growth of large porphyroblasts. These changes would allow a pluton to more easily deform the country rock during emplacement and allow the rapid growth of large porphyroblasts in its aureole. Perhaps it was this fluid rich environment that allowed Late Cretaceous plutons to more easily deform and metamorphose their country rock and form these types of gneiss dome culminations.

## References

- Ahlborn, R. C. (1977). Mesozoic-Cenozoic Structural Development of the Kern Mountains, Eastern Nevada-Western Utah. *Brigham Young University Geology Studies*, 24(2), 117-131.
- Armstrong, R. L. (1968). Sevier orogenic belt in Nevada and Utah. *Geological Society of America Bulletin*, 79(4), 429-458.0. [https://doi.org/10.1130/0016-7606\(1968\)79\[429:SOBINA\]2.0.CO;2](https://doi.org/10.1130/0016-7606(1968)79[429:SOBINA]2.0.CO;2)
- Barton, M. D., & Anderson, J. L. (1990). Cretaceous magmatism, metamorphism, and metallogeny in the east-central Great Basin. *The nature and origin of Cordilleran magmatism: Geological Society of America Memoir*, 174, 283-302.
- Best, M. G., Armstrong, R. L., Graustein, W. C., Embree, G. F., & Ahlborn, R. C. (1974). Mica granites of the Kern Mountains pluton, eastern White Pine County, Nevada: Remobilized basement of the Cordilleran miogeosyncline?. *Geological Society of America Bulletin*, 85(8), 1277-1286. [https://doi.org/10.1130/0016-7606\(1974\)85<1277:MGOTKM>2.0.CO;2](https://doi.org/10.1130/0016-7606(1974)85<1277:MGOTKM>2.0.CO;2)
- Bick, K. F. (1966). Geology of the Deep Creek Mountains, Tooele and Juab Counties, Utah. *Utah Geological and Mineralogical Survey Bulletin*, 77.
- Caggianelli, A., Ranalli, G., Lavecchia, A., Liotta, D., & Dini, A. (2014). Post-emplacement thermo-rheological history of a granite intrusion and surrounding rocks: the Monte Capanne pluton, Elba Island, Italy. *Geological Society, London, Special Publications*, 394(1), 129-143. <https://doi.org/10.1144/SP394.1>
- Camilleri, P. A., & Chamberlain, K. R. (1997). Mesozoic tectonics and metamorphism in the Pequop Mountains and Wood Hills region, northeast Nevada: Implications for the architecture and evolution of the Sevier orogen. *Geological Society of America Bulletin*, 109(1), 74-94. [https://doi.org/10.1130/0016-7606\(1997\)109<0074:MTAMIT>2.3.CO;2](https://doi.org/10.1130/0016-7606(1997)109<0074:MTAMIT>2.3.CO;2)
- Clemens, J. D., & Mawer, C. K. (1992). Granitic magma transport by fracture propagation. *Tectonophysics*, 204(3-4), 339-360. [https://doi.org/10.1016/0040-1951\(92\)90316-X](https://doi.org/10.1016/0040-1951(92)90316-X)
- Cruz-Uribe, A. M., Hoisch, T. D., Wells, M. L., Vervoort, J. D., & Mazdab, F. K. (2015). Linking thermodynamic modelling, Lu-Hf geochronology and trace elements in garnet: New P-T-t paths from the Sevier hinterland. *Journal of Metamorphic Geology*, 33(7), 763-781. <https://doi.org/10.1111/jmg.12151>
- DeCelles, P. G., & Coogan, J. C. (2006). Regional structure and kinematic history of the Sevier fold-and-thrust belt, central Utah. *Geological Society of America Bulletin*, 118(7-8), 841-864. <https://doi.org/10.1130/B25759.1>

Douce, P., Humphreys, E. D., & Johnston, A. D. (1990). Anatexis and metamorphism in tectonically thickened continental crust exemplified by the Sevier hinterland, western North America. *Earth and Planetary Science Letters*, 97(3), 290-315.  
[https://doi.org/10.1016/0012-821X\(90\)90048-3](https://doi.org/10.1016/0012-821X(90)90048-3)

Farmer, G. L., & DePaolo, D. J. (1983). Origin of Mesozoic and Tertiary granite in the western United States and implications for Pre-Mesozoic crustal structure: 1. Nd and Sr isotopic studies in the geocline of the Northern Great Basin. *Journal of Geophysical Research: Solid Earth*, 88(B4), 3379-3401. <https://doi.org/10.1029/JB088iB04p03379>

Glazner, A. F., Bartley, J. M., Coleman, D. S., Gray, W., & Taylor, R. Z. (2004). Are plutons assembled over millions of years by amalgamation from small magma chambers?. *GSA today*, 14(5-Apr), 4-11. <https://doi.org/10.17615/nspy-zk53>

Gottlieb, E. S., Miller, E. L., Valley, J. W., Fisher, C. M., Vervoort, J. D., & Kitajima, K. (2022). Zircon petrochronology of Cretaceous Cordilleran interior granites of the Snake Range and Kern Mountains, Nevada, USA. In J. P. Craddock et al. (Eds.), *Tectonic Evolution of the Sevier-Laramide Hinterland, Thrust Belt, and Foreland, and Postorogenic Slab Rollback (180–20 Ma)*, GSA Special Bulletin (Vol. 555, pp. 21-65). Boulder, CO: Geological Society of America. [https://doi.org/10.1130/2022.2555\(02\)](https://doi.org/10.1130/2022.2555(02))

Harrison, T. M., & Clarke, G. K. (1979). A model of the thermal effects of igneous intrusion and uplift as applied to Quattoon pluton, British Columbia. *Canadian Journal of Earth Sciences*, 16(3), 411-420. <https://doi.org/10.1139/e79-03>

Hirth, G., & Tullis, J. A. N. (1992). Dislocation creep regimes in quartz aggregates. *Journal of structural geology*, 14(2), 145-159. [https://doi.org/10.1016/0191-8141\(92\)90053-Y](https://doi.org/10.1016/0191-8141(92)90053-Y)

Horstwood, M. S., Foster, G. L., Parrish, R. R., Noble, S. R., & Nowell, G. M. (2003). Common-Pb corrected in situ U–Pb accessory mineral geochronology by LA-MC-ICP-MS. *Journal of Analytical Atomic Spectrometry*, 18(8), 837-846.  
<https://doi.org/10.1039/B304365G>

Horstwood, M. S., Košler, J., Gehrels, G., Jackson, S. E., McLean, N. M., Paton, C., et al. (2016). Community-derived standards for LA-ICP-MS U-(Th-) Pb geochronology—Uncertainty propagation, age interpretation and data reporting. *Geostandards and Geoanalytical Research*, 40(3), 311-332. <https://doi.org/10.1111/j.1751-908X.2016.00379.x>

Hose, R. K., & Blake, M. C. (1976). Geology of White Pine County, Nevada. *Nevada Bureau of Mines and Geology Bulletin*, 85, 1-35.

Hutton, D. H. (1996). The 'space problem' in the emplacement of granite. *Episodes Journal of International Geoscience*, 19(4), 114-119.  
<https://doi.org/10.18814/epiugs/1996/v19i4/004>

- Kelly, E. D., Hoisch, T. D., Wells, M. L., Vervoort, J. D., & Beyene, M. A. (2015). An Early Cretaceous garnet pressure–temperature path recording synconvergent burial and exhumation from the hinterland of the Sevier orogenic belt, Albion Mountains, Idaho. *Contributions to Mineralogy and Petrology*, 170, 1-22. <https://doi.org/10.1007/s00410-015-1171-2>
- Kylander-Clark, A. R., Hacker, B. R., & Cottle, J. M. (2013). Laser-ablation split-stream ICP petrochronology. *Chemical Geology*, 345, 99-112. <https://doi.org/10.1016/j.chemgeo.2013.02.019>
- Lee, D. E., Kistler, R. W., Friedman, I., & Van Loenen, R. E. (1981). Two-mica granites of northeastern Nevada. *Journal of Geophysical Research: Solid Earth*, 86(B11), 10607-10616. <https://doi.org/10.1029/JB086iB11p1060>
- Lee, D. E., & Christiansen, E. H. (1983). The granite problem as exposed in the southern Snake Range, Nevada. *Contributions to Mineralogy and Petrology*, 83(1-2), 99-116. <https://doi.org/10.1007/BF00373083>
- Lee, S. Y., Barnes, C. G., Snoke, A. W., Howard, K. A., & Frost, C. D. (2003). Petrogenesis of Mesozoic, peraluminous granites in the Lamoille Canyon area, Ruby Mountains, Nevada, USA. *Journal of Petrology*, 44(4), 713-732. <https://doi.org/10.1093/petrology/44.4.713>
- McGrew, A. J., Peters, M. T., & Wright, J. E. (2000). Thermobarometric constraints on the tectonothermal evolution of the East Humboldt Range metamorphic core complex, Nevada. *Geological Society of America Bulletin*, 112(1), 45-60. [https://doi.org/10.1130/0016-7606\(2000\)112<45:TCOTTE>2.0.CO;2](https://doi.org/10.1130/0016-7606(2000)112<45:TCOTTE>2.0.CO;2)
- Miller, C. F., & Bradfish, L. J. (1980). An inner Cordilleran belt of muscovite-bearing plutons. *Geology*, 8(9), 412-416. [https://doi.org/10.1130/0091-7613\(1980\)8<412:AICBOM>2.0.CO;2](https://doi.org/10.1130/0091-7613(1980)8<412:AICBOM>2.0.CO;2)
- Miller, E. L., & Gans, P. B. (1989). Cretaceous crustal structure and metamorphism in the hinterland of the Sevier thrust belt, western US Cordillera. *Geology*, 17(1), 59-62. [https://doi.org/10.1130/0091-7613\(1989\)017<0059:CCSAM>2.3.CO;2](https://doi.org/10.1130/0091-7613(1989)017<0059:CCSAM>2.3.CO;2)
- Miller, E. L., Gans, P. B., Wright, J. E., Sutter, J. F., & Ernst, W. G. (1988). Metamorphic history of the east-central Basin and Range province: Tectonic setting and relationship to magmatism. *Metamorphism and crustal evolution, western conterminous United States, Rubey*, 7, 649-682.
- Miller, R. B., & Paterson, S. R. (1999). In defense of magmatic diapirs. *Journal of Structural Geology*, 21(8-9), 1161-1173. [https://doi.org/10.1016/S0191-8141\(99\)00033-4](https://doi.org/10.1016/S0191-8141(99)00033-4)

Monroe E. B., Kylander-Clark, A. R., & Gans, P. B. (2023a). U-Pb zircon geochronology of the Trout Creek Intrusive Complex, Deep Creek Range, UT [Dataset]. Harvard Dataverse. <https://doi.org/10.7910/DVN/GBUGGX>

Monroe E. B., Kylander-Clark, A. R., & Gans, P. B. (2023b). U-Pb monazite geochronology of the Trout Creek schist, Deep Creek Range, UT [Dataset]. Harvard Dataverse. <https://doi.org/10.7910/DVN/SP4UXM>

Nutt, C. J., & Thorman, C. H. (1994). *Geologic Map of the Weaver Canyon, Nevada and Utah, Quadrangle and Parts of the Ibapah Peak, Utah, and Tippett Canyon, Nevada, Quadrangles* (No. 94-635). Denver, CO: US Geological Survey.

<https://doi.org/10.3133/ofr94635>

Palin, R. M., Searle, M. P., Waters, D. J., Parrish, R. R., Roberts, N. M. W., Horstwood, M. S., et al. (2013). A geochronological and petrological study of anatetic paragneiss and associated granite dykes from the Day Nui Con Voi metamorphic core complex, North Vietnam: constraints on the timing of metamorphism within the Red River shear zone. *Journal of Metamorphic Geology*, 31(4), 359-387. <https://doi.org/10.1111/jmg.12025>

Paterson, S. R., & Farris, D. W. (2008). Downward host rock transport and the formation of rim monoclines during the emplacement of Cordilleran batholiths. *Earth and Environmental Science Transactions of The Royal Society of Edinburgh*, 97(4), 397-413.

<https://doi.org/10.1017/S026359330000153X>

Paterson, S. R., & Fowler Jr, T. K. (1993). Extensional pluton-emplacement models: Do they work for large plutonic complexes?. *Geology*, 21(9), 781-784.

[https://doi.org/10.1130/0091-7613\(1993\)021<0781:EPEMDT>2.3.CO;2](https://doi.org/10.1130/0091-7613(1993)021<0781:EPEMDT>2.3.CO;2)

Paton, C., Hellstrom, J., Paul, B., Woodhead, J., & Hergt, J. (2011). Iolite: Freeware for the visualisation and processing of mass spectrometric data. *Journal of Analytical Atomic Spectrometry*, 26(12), 2508-2518. <https://doi.org/10.1039/C1JA10172B>

Rodgers, D. W. (1987). *Thermal and structural evolution of the southern Deep Creek Range, west central Utah and east central Nevada* (Doctoral dissertation). Stanford, CA: Stanford University.

Sláma, J., Košler, J., Condon, D. J., Crowley, J. L., Gerdes, A., Hanchar, J. M., et al. (2008). Plešovice zircon—a new natural reference material for U-Pb and Hf isotopic microanalysis. *Chemical Geology*, 249(1-2), 1-35. <https://doi.org/10.1016/j.chemgeo.2007.11.005>

Spear, F. S. (1993). *Metamorphic phase equilibria and pressure-temperature-time paths*. Chantilly, VA: Mineralogical Society of America Monograph.

Taylor, W. J., Bartley, J. M., Martin, M. W., Geissman, J. W., Walker, J. D., Armstrong, P. A., & Fryxell, J. E. (2000). Relations between hinterland and foreland shortening: Sevier

orogeny, central North American Cordillera. *Tectonics*, 19(6), 1124-1143.  
<https://doi.org/10.1029/1999TC001141>

Teyssier, C., & Whitney, D. L. (2002). Gneiss domes and orogeny. *Geology*, 30(12), 1139-1142. [https://doi.org/10.1130/0091-7613\(2002\)030<1139:GDAO>2.0.CO;2](https://doi.org/10.1130/0091-7613(2002)030<1139:GDAO>2.0.CO;2)

Tomascak, P. B., Krogstad, E. J., & Walker, R. J. (1996). U-Pb monazite geochronology of granitic rocks from Maine: implications for late Paleozoic tectonics in the Northern Appalachians. *The Journal of Geology*, 104(2), 185-195. <https://doi.org/10.1086/629813>

Wiedenbeck, M. A. P. C., Alle, P., Corfu, F. Y., Griffin, W. L., Meier, M., Oberli, et al. (1995). Three natural zircon standards for U-Th-Pb, Lu-Hf, trace element and REE analyses. *Geostandards newsletter*, 19(1), 1-23.  
<https://doi.org/10.1111/j.1751-908X.1995.tb00147.x>

Wright, J. E., & Wooden, J. L. (1991). New Sr, Nd, and Pb isotopic data from plutons in the northern Great Basin: Implications for crustal structure and granite petrogenesis in the hinterland of the Sevier thrust belt. *Geology*, 19(5), 457-460.  
[https://doi.org/10.1130/0091-7613\(1991\)019<0457:NSNAPI>2.3.CO;2](https://doi.org/10.1130/0091-7613(1991)019<0457:NSNAPI>2.3.CO;2)

Yoshinobu, A. S., Okaya, D. A., & Paterson, S. R. (1998). Modeling the thermal evolution of fault-controlled magma emplacement models: implications for the solidification of granitoid plutons. *Journal of Structural Geology*, 20(9-10), 1205-1218.  
[https://doi.org/10.1016/S0191-8141\(98\)00064-9](https://doi.org/10.1016/S0191-8141(98)00064-9)